Computational Screening and Multiscale Simulation of Barrier-Free Contacts for 2D Semiconductor pFETs

Ning Yang¹, Yuxuan Cosmi Lin^{1*}, Chih-Piao Chuu², Saifur Rahman³, Tong Wu⁴, Ang-Sheng Chou², San-Lin Liew⁵, Kohei Fujiwara⁶, Hung-Yu Chen¹, Junya Ikeda⁶, Atsushi Tsukazaki⁶, Duen-Huei Hou⁵, Wei-Yen Woon⁷, Szuya Liao⁷, Shengxi Huang^{3,8}, Xiaofeng Qian⁹, Jing Guo⁴, Iuliana Radu², H.-S. Philip Wong², Han Wang^{1*}

¹Corporate Research, TSMC, San Jose, CA, USA; ²Corporate Research, TSMC, Hsinchu, Taiwan; ³Electrical Engineering, Pennsylvania State University, State College, PA, USA; ⁴Electrical and Computer Engineering, University of Florida, Gainesville, FL, USA; ⁵Quality & Reliability, TSMC, Hsinchu, Taiwan; ⁶Institute for Materials Research, Tohoku University, Sendai, Japan; ⁷Pathfinding, TSMC, Hsinchu, Taiwan; ⁸Electrical and Computer Engineering, Rice University, Houston, TX, USA; ⁹Materials Science and Engineering, Texas A&M University, College Station, TX, USA; *Email: cosmil@tsmc.com; hanwang@tsmc.com

Abstract - Low-resistance p-type contacts to two-dimensional (2D) semiconductors remains a critical challenge towards the industrial application of 2D channel materials in advanced logic technology. To address this challenge, we computationally screen and identify designs for ultralow-resistance p-type contacts to 2D semiconductors such as WSe2 by combining ab initio densityfunctional-theory (DFT) and quantum device simulations. Two new contact strategies, van der Waals metallic contact (such as 1H-NbS₂), and bulk semimetallic contact (such as Co₃Sn₂S₂), are identified as realistic pathways to achieving Schottky-barrier-free and low-contact-resistance p-type contacts for 2D semiconductor pFETs. Simulations of these new strategies suggest reduced metal-induced gap states, negligible Schottky barrier height and small contact resistance (down to ~20 Ω·μm). Preliminary experimental results in developing Co₃Sn₂S₂ as a new semimetal contact material are also demonstrated.

I. INTRODUCTION

2D semiconducting transition-metal dichalcogenides (TMDs), such as MoS₂, WS₂ and WSe₂, are potential candidates for future field effect transistor (FET) technology with sub-10 nm gate lengths and sub-2-nm body thickness (Fig. 1) [1]. However, making low resistance contacts for 2D semiconductor p-type FET (pFET) is among the most critical bottlenecks hindering the practical application of 2D channel materials in advanced CMOS logic nodes. Previous work has demonstrated that low density-ofstates (DOS) semimetals, including Bi, and Sb, can address the metal-induced gap states (MIGS) issue for 2D TMDs, and recordhigh n-type FET (nFET) performance has been reported [2-5]. However, these semimetals may not be suitable for the metallic contacts of pFET due to their relatively low work functions (WFs) and hence the large energy mismatch between the WFs of these semimetals and the hole affinities of 2D TMDs. An essential pathway to barrier-free p-type contact is to search for high WF metallic materials with reduced or eliminated MIGS. In this work, we report the first systematic computational study of high workfunction semimetals and van der Waals (vdW) metals that can form barrier-free contacts for 2D pFETs. The key contribution of this work is four-folds: (i) This work exemplifies a wide range of bulk topological semimetals and vdW metal materials, and their transport properties when in contact with 2D TMDs through computational approaches. Monolayer WSe2 (will be referred to as WSe₂ from now on) is selected in this study because of it relatively low hole affinity. (ii) Several high WF materials are identified for the first time as promising candidates for contacting 2D pFET, especially the topological semimetal Co₃Sn₂S₂, and vdW metallic materials 1T-TiS₂. Preliminary experimental development and characterization $\text{Co}_3\text{Sn}_2\text{S}_2$ as a topological semimetal contact material is also presented. (iii) Simulations of these new contact approaches revealed reduced MIGS and negligible Schottky barrier height (SBH) and the potential to achieve theoretical contact resistance (R_{C}) as low as 20 $\Omega \cdot \mu \text{m}$. (iv) A multi-scale simulation framework is utilized to evaluate the performance potential of 2D pFETs based on new contact options such as $\text{Co}_3\text{Sn}_2\text{S}_2$.

II. APPROACH

Density-functional-theory (DFT) simulations were conducted by Vienna Ab-initio Simulation Package (VASP). Projector augmented wave (PAW) method and Perdew-Burke-Ernzerhof (PBE) exchange-correlation energy functional within the generalized gradient approximation (GGA) were used. DFT-D2 method was utilized to treat the weak vdW interactions. Supercell structures were built to ensure the small lattice mismatches between WSe₂ and metal/semimetal (<2%). The cutoff energy for the plane-wave-basis was set to be 520 eV. The Brillouin zone was sampled by Monkhorst-Pack scheme, where the number of mesh points in z-direction is 1 and the numbers of mesh points in x-y plane depend on different supercell structures. The band structures were generated based on the unit cell for 1H-NbS₂-WSe₂ stack and supercells for Co₃Sn₂S₂/WSe₂ [6] and Pt/WSe₂ interfaces. In the simulation of heterostructures, vdW materials had monolayer structure, bulk semimetals had one unit-cell in the z-direction, and conventional metals were stacked on the (111) surfaces.

Further analysis based on DFT calculations were performed with full relaxations of the atomistic structures. The interlayer distance (d) was extracted when total energy was minimized. Dipole corrections to the total energy were conducted in the WF calculations of heterojunctions. The interface dipole (ID) density was obtained from the WF difference between WSe₂ and the metallic material (Δ WF), expressed as ID density= $\varepsilon_0\Delta$ WF/(ed), where ε_0 is the vacuum permittivity, and e is the electron charge. The binding energy of interface (E_0) is the energy difference before and after the formation of the heterojunctions. The total MIGS values were calculated by the integral of the partial local density of states (PLDOS) of WSe₂ within the bandgap. P-type (n-type) Schottky barrier heights, pSBH (nSBH), were the energy difference between the Fermi levels and the valence band maximum, VBM (conduction band minimum, CBM) of WSe₂.

 R_c of the Schottky-barrier (SB) -free contacts was computed through an analytical model incorporated with the DFT results [2]. The theoretical limit was estimated through a novel multiscale method recently developed for n-type contacts that integrates DFT simulation results with tight-binding quantum transport (non-equilibrium Green's function, NEGF) simulations [7]. R_c for SB-

limited contacts were computed through the Landauer formula with considerations of both the thermionic emission and tunneling across the SB. The I-V characteristics were obtained by combining the computed R_c and the I-V for the WSe₂ channel resolved by the NEGF simulation and self-consistent 2D Poisson's equation [9]. Ballistic transport model was used.

III. RESULTS

A. Ab initio DFT Simulations of WSe₂ P-Type Contacts

Three types of metallic materials are investigated as p-type contacts to WSe2 (Fig. 2), including: (1) strategy I: 2D vdW metallic materials such as 1T-TiS2, 1H-NbS2, 1T-NbS2 and 1T'-WTe2; (2) strategy II: bulk topological semimetals such as Co₃Sn₂S₂, TaP, and LaBi; and (3) conventional metals such as Pt, Pd, Au, Ag and Al as the control group. Both high-WF vdW metallic materials (strategy I) and high-WF bulk semimetals (strategy II) are good candidates for WSe₂ p-type contact according to DFT simulations. Here we take $1H-NbS_2$ (strategy I, WF = 6.11 eV), Co₃Sn₂S₂ (strategy II WF = 5.32 eV), and Pt (conventional, WF = 5.7 eV) as examples (Fig. 3). Because of the weak vdW coupling at the interface between WSe2 and the vdW contact (1H-NbS₂), and the low DOS around the Fermi level of the bulk semimetal contact (Co₃Sn₂S₂), the interactions between WSe₂ and these two contact materials are extremely weak compared to conventional metals, leading to much smaller MIGS and less pinning effect (Fig. 4). pSBH can be completely eliminated if the metal WF is higher than the hole affinity (4.9 eV for WSe₂). The great reduction of electronic band re-hybridizations for 1H-NbS₂/WSe₂ and Co₃Sn₂S₂/WSe₂ heterojunctions can be visualized by the color-coded band structures (Fig. 4a and b). The final Fermi levels are around the VBM, indicating eliminated pSBH. As a comparison, the band structure of high-WF conventional metal contact such as Pt/WSe2 shows high MIGS, leading to strong Fermi level pinning and large pSBH (Fig. 4c).

B. Computational Screening of P-Type Contact Materials

WFs for various vdW and bulk semimetal contact materials are computed (Fig. 5). WFs higher than 4.9 eV are suitable for p-type contacts for WSe₂, and WFs higher than 5.8 eV are good for WS₂ and MoS₂. For vdW metallic materials, only single WFs are recorded, whereas for some of the bulk semimetals, multiple WFs are recorded, corresponding to different surface terminations. For example, to obtain a good surface contact between topological semimetal Co₃Sn₂S₂ and WSe₂, sulfur-terminated surface with the WF of 5.3eV is chosen in the DFT simulation. In another example, tantalum-terminated TaP (denoted as TaP(Ta)) has lower surface WF than phosphorus-terminated TaP (TaP (P)).

Multiple physical parameters extracted from DFT simulations at the contact interfaces are analyzed, offering fundamental understanding about the proposed contact strategies. In Fig. 6a, WFs of WSe₂ after in contact with different types of metallic materials with different WFs are compared. High-WF vdW and semimetal contacts induce large Fermi level shifts and bring the WFs of the heterojunctions closer to the original WFs of the metallic materials which is also close to the VBM of WSe₂, while WFs of conventional metals have less impact on the final WFs which are farther away from the VBM. To characterize the interface interactions, interlayer distances, ID densities, and E_b are extracted, as shown in Fig. 6b,c and Fig. 7a. Interlayer distances smaller than 3 Angstrom (Å), ID densities closer to zero, and E_b smaller than 50 meV/Å² are observed for all the computed high-

WF vdW and semimetal contacts, whereas opposite trends are found for conventional metal contacts. Next, the dramatic reduction of MIGS for the high-WF vdW and semimetallic contacts are observed which is indicated by the total MIGS states in Fig. 7b. Note that the lower-WF termination for the same contact material (TaP(Ta) as an example) leads to stronger interface interactions and higher total MIGS as compared to the higher WF terminations (TaP(P)), which can be attributed to either larger electron orbital overlaps of different chemical elements, or increased DOS at the WSe₂ VBM. In addition, different stacking orders (AA and AB) between the vdW contact and WSe2 has minimal impact on the interface interaction strengths and the final band alignments. Finally, Fig. 7c summarizes the extracted pSBH and nSBH. The pinning factors (the slope of each material group) are ~0.5 for both vdW and semimetallic contact strategies, much larger than those of conventional metal contacts (~0.05), suggesting a greatly reduced Fermi level pinning effect. Experimental results from literature [8] are also included, in good agreement with simulations. All the simulated high-WF vdW materials and bulk semimetals exhibit negligible pSBHs, including 1H-NbS₂, 1T-NbS₂, and 1T-TiS₂ in the vdW material category, as well as Co₃Sn₂S₂ and TaP(P) in the bulk semimetal category.

C. Experimental Characterization of Co₃Sn₂S₂

To demonstrate the experimental feasibility of the proposed contact strategies, we take $\text{Co}_3\text{Sn}_2\text{S}_2$ as an example, which is identified as the most promising candidate among all the bulk topological semimetals (strategy II) studied here to form barrier-free contact for 2D WSe₂ pFET. We show that $\text{Co}_3\text{Sn}_2\text{S}_2$ can be experimentally synthesized through sputtering on sapphire substrates followed by a high-temperature annealing process (800°C). Cross-sectional high-resolution scanning transmission electron microscope (HR-STEM), the associated energy dispersive X-ray spectroscopy (EDX), Raman spectroscopy, and X-ray diffraction (XRD) results as shown in Fig. 8 and 9 indicate the expected chemical composition and crystalline structure.

D. Multiscale Simulation and Device Performance Projection

A multiscale simulation framework is developed to project the $R_{\rm C}$ and device performance of the proposed p-type contact strategies. Three components need to be considered at the contact, including the tunneling resistivity around the metal-WSe2 interface (ρ_t) , the sheet resistance of WSe₂ at the contact (R_{SHC}) , as well as the lateral SB resistance (R_{SB}), if any, as shown in Fig. 10. Fig. 11a plot the simulated $R_{\rm C}$ and transfer length $L_{\rm T}$ for the high-WF vdW and semimetal materials. R_C of 20-100 Ω ·µm and L_T of 3-13 nm can be achieved depending on the quality of WSe2 when in contact with these metals. R_C versus WSe₂ mobility is plotted in Fig. 11b to better display the material quality dependence. $R_{\rm C}$ down to ~20 Ω ·µm can be achieved, approaching the quantum limit. As a reference the best reported p-type R_C value from experiment is ~0.95 kΩ·μm [10]. I-V characteristics of a double-gated WSe₂ pFET with Co₃Sn₂S₂ contacts (53 Ω·μm), 3nm thick HfO₂ gate dielectrics, and 10-30 nm gate lengths (L) are simulated (Fig. 12). On-state current of ~ 2 mA/ μ m at $V_{DS} = -0.5$ V is projected.

Reference: [1] S. Das, et al., Nat. Electron. 4, 786 (2021). [2] P.-C. Shen, et al., Nature 593, 211 (2021). [3] Y. Lin, et al., IEDM, 37.2.1 (2021). [4] A.-S. Chou, et al., IEDM, 7.2.1 (2021). [5] K.P. O'Brien, et al., IEDM, 7.1.1 (2021). [6] Y. Xing, et al. Nat. Commun. 11, 5613 (2020). [7] T. Wu, et al., Appl. Phys. Lett., 121, 023507 (2022). [8] J. Jang, et al., Adv. Mater. 34, 2109899 (2022). [9] Z. Dong et al., IEEE TED, 64, 622 (2017). [10] C.-C. Chiang, et al., IEEE EDL, 43, 319 (2022).

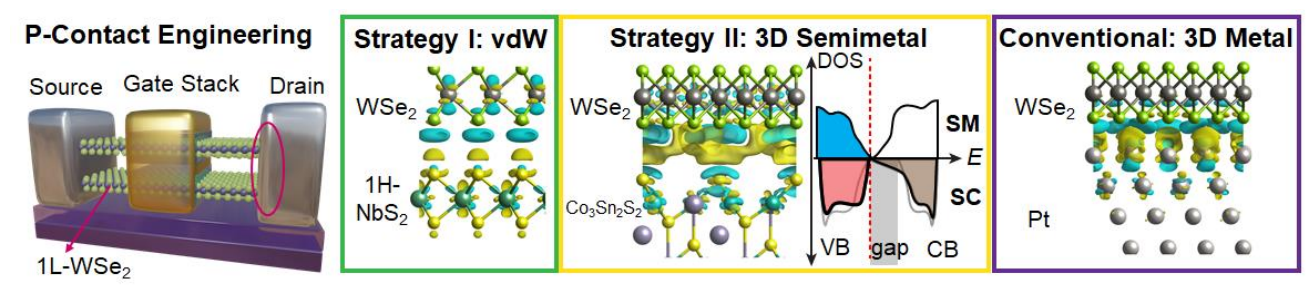


Fig. 1. Schematic of a monolayer WSe₂ nanosheet transistor. Finding a barrierless p-type contact is the goal of this work.

Fig. 2. Strategies for p-type WSe₂ contact: 2D vdW materials, 3D bulk semimetals, and conventional 3D metals. The side view of atomistic structures and the differential charge density of heterojunctions are shown (yellow: positive, blue: negative). 3D semimetals have low MIGS due to low DOS at Fermi level.

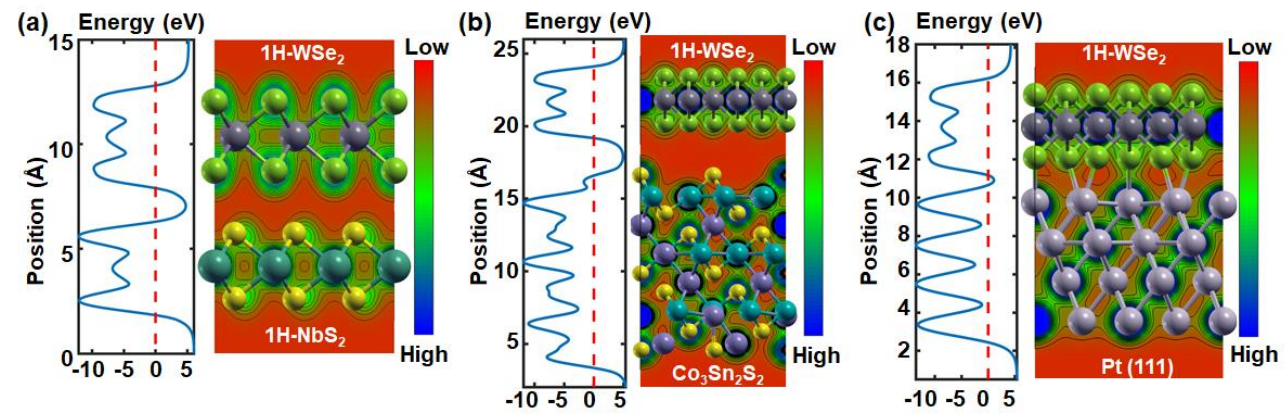


Fig. 3. Cross-sectional view of simulated interface charge density and electrostatic potential profiles of heterostructures: (a) 1H-NbS₂ with 1H-WSe₂ (b) Sulfur-terminated Co₃Sn₂S₂ with 1H-WSe₂ (c) Pt(111) with 1H-WSe₂, each representing the 3 contact cases: 2D vdW materials, 3D bulk semimetal and 3D conventional metals, respectively.

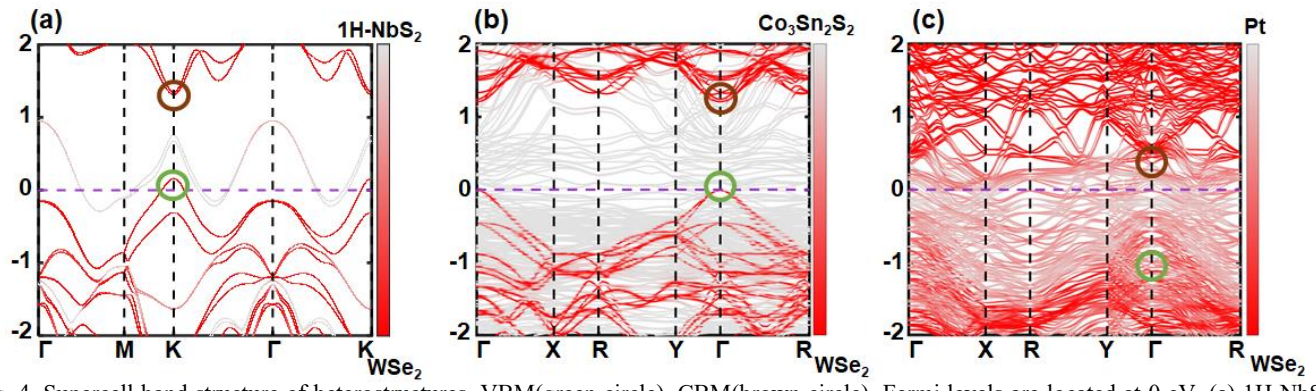


Fig. 4. Supercell band structure of heterostructures, VBM(green circle), CBM(brown circle), Fermi levels are located at 0 eV. (a) 1H-NbS2 with 1H-WSe2 (b) Sulfur-terminated Co₃Sn₂S₂ with 1H-WSe₂ (c) Pt(111) with 1H-WSe₂. The curves are color coded acording to the origins of the states: red color for WSe₂ and grey color for the contact materials 1H-NbS₂, Co₃Sn₂S₂ and Pt.

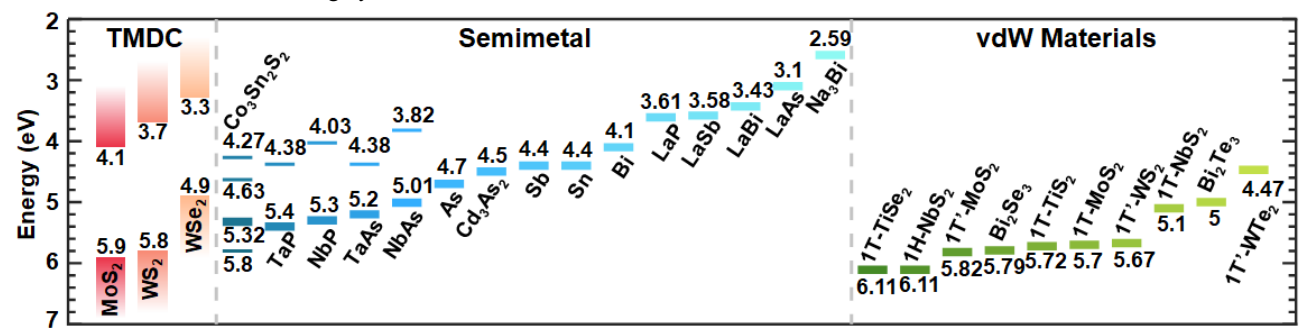


Fig. 5. Calculated CBMs and VBMs for TMDs and WFs of bulk semimetals and multilayer 2D vdW materials. Some semimetals have different surface terminations: Co₃Sn₂S₂ has 4 surfaces: 5.8eV and 5.32eV for sulfur-termination, 4.63 eV for Co₃Sn termination and 4.27 eV for Co termination. For TaP, NbP, TaAs and TaP, surfaces of non-metal elements have higher work functions and surfaces of metal elements have lower work functions. S-terminated Co₃Sn₂S₂ (5.32 eV), P-terminated TaP (5.4 eV), 1T-NbS₂, 1T-TiS₂ and 1H-NbS₂ are used in subsequent study to construct metal/WSe₂ contact heterostructures.

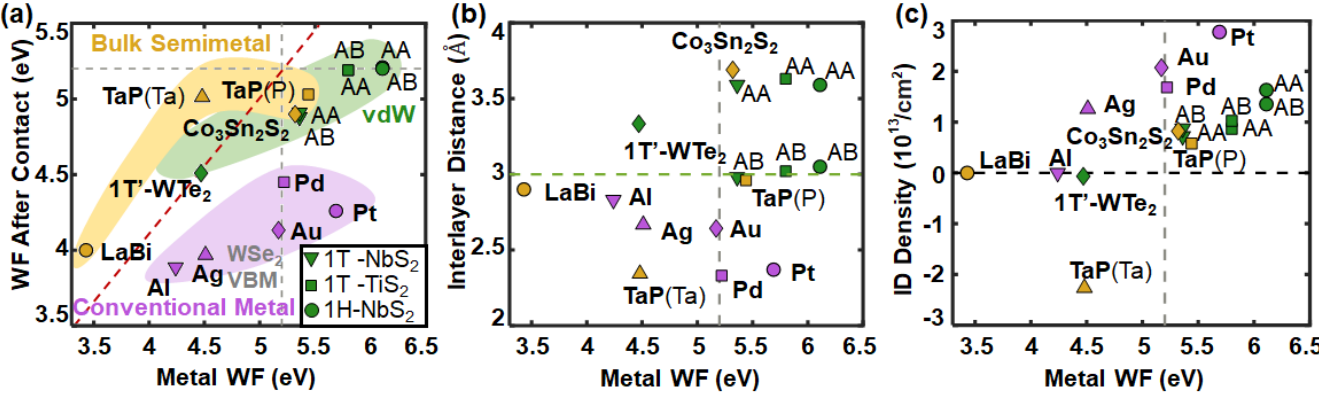


Fig. 6. (a) WF of WSe₂ after contact, (b) interlayer distance, and (c) interlayer dipole (ID) density versus pristine metal WF. VBM of WSe₂ is marked in gray. AA, AB mean stacking of vdW metal/WSe₂ heterostructures. <u>Labels for (b, c), Fig. 7, and Fig. 11 follow the same as (a).</u> Red dotted line in (a) corresponds to the same WF of WSe₂ after contact as the WF of pristine metal.

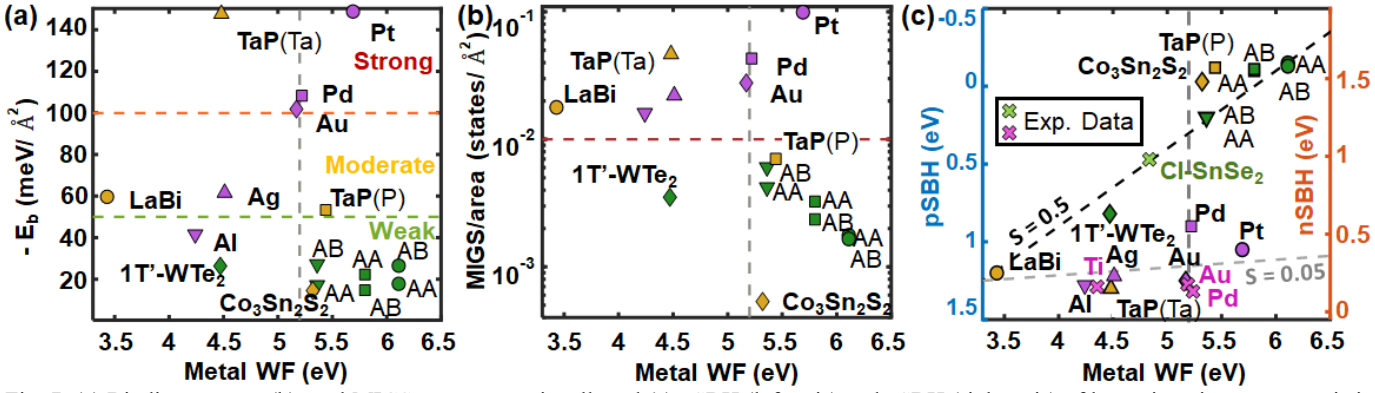


Fig. 7. (a) Binding energy, (b) total MIGS states per unit cell, and (c) pSBH (left axis) and nSBH (right axis) of heterojunctions versus pristine metal WF. For (c), experimental results from [8] are marked as crosses showing remarkable agreement with simulation results. The dashed lines with slopes of 0.5 and 0.05 correspond to vdW and semimetalic contacts with weak pinning, and conventional metal with strong pinning in (c).

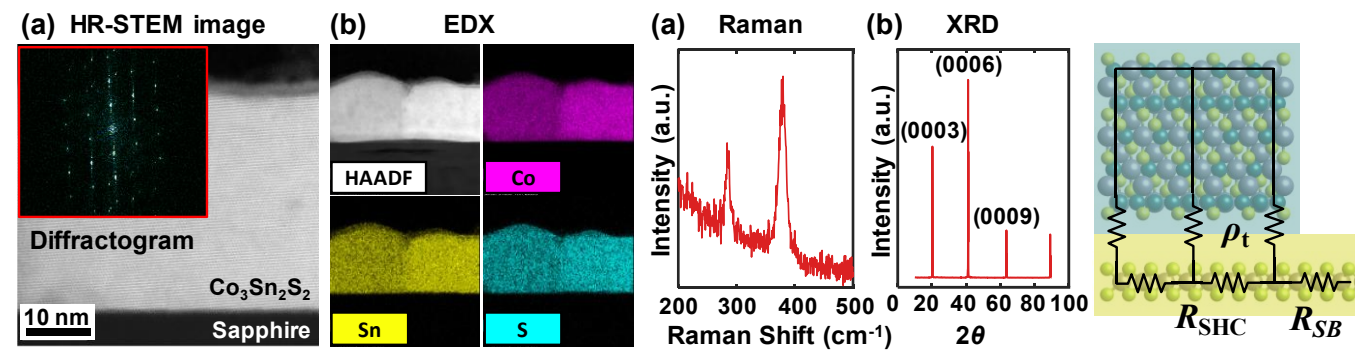


Fig. 8. (a) cross-sectional HR-STEM image of an experimental crystalline Co₃Sn₂S₂ film obtained in this work. Inset: the experimental corresponding diffractogram. (b) EDX of the film.

Fig. 9. (a) Raman and (b) XRD of the experimental Co₃Sn₂S₂ crystal.

Fig. 10. Schemetic of the model at the contact.

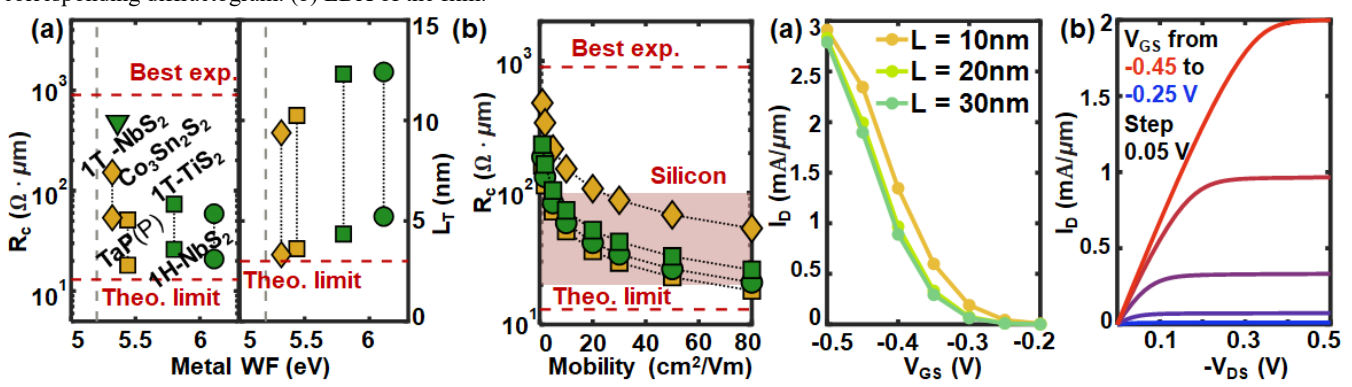


Fig. 11. (a) $R_{\rm C}$ (left) and $L_{\rm T}$ (right) versus pristine metal WF. Two cases of WSe₂ mobilities of 10 cm²V⁻¹S⁻¹ and 80 cm²V⁻¹S⁻¹ (linked by dotted line) under the contact are simulated. $R_{\rm C}$ for 1T-NbS₂ has no mobility dependence, because it is limited by $R_{\rm SB}$ in Fig. 10. (b) $R_{\rm C}$ versus WSe₂ mobility under the contact. Best experiment [10], theoretical limit, and $R_{\rm C}$ for Si are also marked.

Fig. 12. (a) Simulated transfer characteristics with different gate lengths, L, and $V_{\rm DS} = -0.5$ V. (b) Simulated output characteristics at L=20 nm for Co₃Sn₂S₂/WSe₂ FET.